Single-shot depth-section imaging through chromatic slit-scan confocal microscopy

Paul C. Lin, Pang-Chen Sun, Lijun Zhu, and Yeshaiahu Fainman

A chromatic confocal microscope constructed with a white-light source in combination with a diffractive lens provides wavelength-to-depth coding for profile measurements of a three-dimensional sample. We acquired depth-section images nonmechanically and in parallel by incorporating a slit-scan confocal technique into the system. A system using a 100× objective obtained a depth resolution of 0.023 μm comparable with surface profilometers that operate using conventional confocal microscopy. Experimental measurements of a four-phase-level diffractive element and of a machined, metal bearing are presented. © 1998 Optical Society of America

OCIS codes: 050.1970, 110.0180, 110.6960, 120.6660, 180.1790, 180.6900.

1. Introduction

The need for depth-measurement profilometry devices spans many different fields in science and in industry. The observation of biological specimens, geological samples, fabricated materials, machined parts, integrated circuits, microelectromechanical systems, and diffractive elements can all be aided by surface profile information. One device that allows precise depth measurements is the confocal microscope. This instrument was invented by Minsky in 1957,[1] but most subsequent development occurred in the mid-1980's when it found widespread use in biological applications owing to its ability to localize fluorescence labels accurately within thick, optically transparent specimens.[2] The use of the confocal microscope has also found applications in other fields such as material science and the semiconductor industry.[3] The unique properties of the confocal microscope, notably its providing images with superior resolution[4] and its ability to perform depth-section imaging,[5] have made it an attractive scientific tool. Although image resolution can be improved in the transverse direction, the main advantage of the confocal microscope is its unique property of depth discrimination, enabling high-resolution measurements along the longitudinal or depth direction.

The operation of the confocal microscope[6] is based on the geometric matching of two imaged conjugate focal (confocal) points, one point corresponding to a point source on the sample surface and the other corresponding to a point detector defined by a pinhole aperture. When the confocal condition is achieved, the two imaged focal points coincide in space, giving a maximal signal intensity at the detector. As the sample surface is moved away from the focal plane, both the illuminated spot and the detected spot lose focus, causing light at the detector plane to be broadened. The pinhole filters out the broadened, off-focus scattered light and the detected intensity rapidly decreases. This depth-discrimination feature of the confocal microscope permits relative depth measurements to be performed. Since probing is done without contacting the sample, the measurements are performed noninvasively. Depth-section images are built from the in-focus parts of the sample while the surface of the sample is scanned over.[7] Thus the confocal microscope can be termed a profilometer where surface profiles are rendered from a sequence of images collected as a function of sample depth.

Although current confocal systems are generally limited to, and achieve, a similar resolution, the performance difference between confocal systems can be attributed to the scanning method used. These methods can be separated into two categories: transverse (x, y) and depth (z) scanning. The scanning technique dictates the speed of the measurement, the illumination efficiency, and the accuracy of

The authors are with the Department of Electrical and Computer Engineering, University of California, San Diego, La Jolla, California 92093-0407.

Received 23 March 1998; revised manuscript received 25 June 1998.
0003-6935/98/286764-07$15.00/0
© 1998 Optical Society of America

the microscope. The original and most basic method used is that of mechanical stage scanning. Stage scanning steps the sample itself across the scan space (x, y, z), point by point, and the surface depth topology can be reconstructed later. This technique is conceptually simple and generally very accurate, but mechanical stage scanning is a slow process. Other scanning methods exist that improve overall speed. The most popular for transverse scanning are galvanometer mirrors or acousto-optic deflectors in applying a Raster-scan over the sample surface. Speed is improved over stage scanning, but the Raster-scan is relatively inaccurate and performed serially. Another popular method for transverse scanning is the rotating Nipkow disk.[8] Although the scan rate is improved owing to multiple-point-source illumination, the Nipkow disk suffers from low illumination efficiency and backscatter noise reflected from the disk itself. In conventional confocal microscopy, scanning the sample in depth, movement of the sample stage or the objective lens is usually necessary, limiting the (x, y, z) scan rate.

To improve scanning speed while maintaining the accuracy and the illumination efficiency of the confocal microscope, our goal was to use methods that increased the scan rate by reinstating optical parallelism and by reducing mechanical movement. We selected use of the slit-scan confocal microscope in our profilometer.[9] This method is similar to the point-scan confocal method but is extended in a straight line along one transverse axis (x or y). Two slits can be arranged in the confocal design to serve as an array of point sources and an array of conjugate point detectors. Illumination from the slit source is imaged onto the sample, which is then reimaged to the second slit used as the detector. The light through the second slit can then be imaged onto a linear detector array for detection. The depth-discrimination property of the slit-scan confocal microscope is preserved owing to the rejection of scattered light along the confined axis. Thus the microscope is still capable of performing depth-section imaging, however, with a resolution slightly inferior to that of point-scan confocal microscopy. Nevertheless the scan rate and the illumination efficiency are dramatically improved by the slit-scan method. More important, it can be used in conjunction with the chromatic confocal depth-scanning technique, which is the central feature of our device.

Chromatic depth scanning, which utilizes chromatic dispersion of the objective lens, has been investigated as a solution for eliminating mechanical depth scanning.[10] By chromatic dispersion, different wavelengths are focused to different focal points along the depth axis. Thus nonmechanical depth scanning can be performed with wavelength tuning. Instead of relying on chromatic dispersion from regular refractive lenses, we use a diffractive lens that can provide strong dispersion with a highly linear wavelength-to-depth coding.[11,12] Not only does this allow for a large scanning range in depth, but it also allows for easily characterized depth measurements. In addition, when we use a broadband point source for illumination, multiple focal depths can be scanned at the same time in parallel. One drawback of the diffractive lens is that its numerical aperture (NA) is limited by the minimum feature size available to microfabrication technology. The small NA of the diffractive lens provides a low resolving power, making the lens unsuitable as the objective lens of a microscope, but that can be used as an eyepiece in the microscope.

The combination of slit scanning and chromatic depth scanning allows image data to be acquired in parallel and without the need for mechanical movement. These two techniques can be combined to perform depth-section measurements in a single shot, improving the scanning speed and maintaining high resolution and accuracy. The ability to provide noninvasive, real-time surface profilometry is useful in a variety of applications. For example, in the semiconductor and automotive industries, being able to adjust process control, or to calibrate machining equipment in real time, allows for a quick turnaround time and improved quality with a higher yield.

We present a chromatic slit-scan confocal microscope (CSCM) that achieves this function. Section 2 contains a description of the experimental CSCM apparatus. In Section 3 we characterize the CSCM system, and in Section 4 we provide samples of experimental measurements. Concluding remarks are in Section 5.

2. System Description

A schematic diagram of the CSCM is shown in Fig. 1. A broadband 75-W Xe lamp was used in the microscope as a light source for illumination with multiple wavelengths in parallel. In general, the power spectrum of the source must be measured and used for spectral data calibration to provide a normalized intensity distribution across the working range of the wavelengths. However, to avoid performing this calibration in our experiments, we used a narrow spectral portion of the Xe source that exhibits a uniform power spectrum. We collimated the broadband source and focused it through the input slit by using a cylindrical lens, improving the illumination efficiency of the system. The optical field passing through the input slit is imaged by a combination of refractive lens and diffractive lens. Owing to the dispersive properties of the diffractive lens, the image planes of the slit are wavelength dependent, uniformly distributed along the longitudinal direction. We then telecentrically imaged the wavelength-coded variable foci onto the measured sample by using a coupling lens and a microscope objective (MO) lens. In this setup the input slit was aligned vertically, resulting in a vertical slice of the sample being measured. The diffractive lens used has a 125-mm focal length with $f/4.5$, designed for operation at a wavelength of 600 nm. The diffractive lens is a binary-phase element fabricated by use of electron-beam lithography and chemically assisted ion-beam etching techniques.

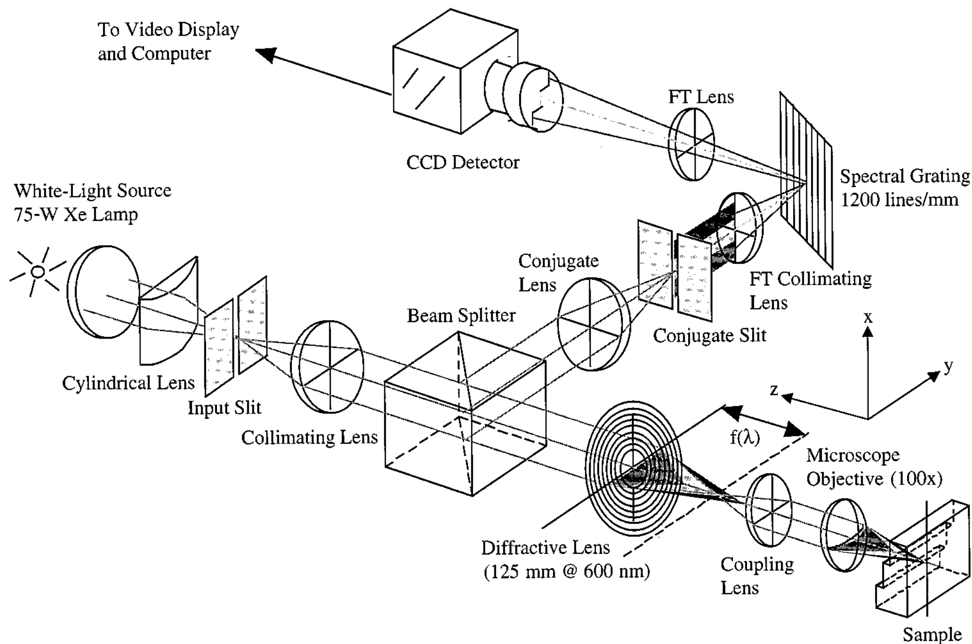

Fig. 1. Schematic diagram of a CSCM with a diffractive lens.

Light reflected from the sample returns through the diffractive lens, but only those wavelengths corresponding to the imaged slit on the sample surface will be recollimated following the same path, to be diverted by a beam splitter and focused through the conjugate slit. The conjugate slit filters out light of all wavelengths scattered from the out-of-focus portions of the sample, thereby providing depth discrimination along a line on the sample as defined by the direction of the slit (the vertical direction in Fig. 1). The light passing through the conjugate slit, corresponding to reflection from the in-focus wavelength-coded illumination, is then coupled into a monochromator, built with two Fourier-transform lenses and a 1200-line/mm spectral grating. The grating is used to disperse spatially the spectrum of the confocal signal along a direction perpendicular to the slit (the horizontal direction in Fig. 1), thereby imaging the conjugate slit to a location on the CCD camera (Pulnix TM-7CN) according to spectral content. In the setup, since the wavelength-coded depth information of the sample is horizontally spread by the spectral grating, the detected CCD image in the horizontal direction is related to the relative surface depth for each position along a vertical line on the sample. Note that along the axis parallel to the slit (the vertical axis in Fig. 1) the optical setup directly images a line on the sample to the CCD detector. With this technique a depth-section profile of the sample surface is captured in a single shot, where a one-dimensional transverse image (i.e., the image of a sample along the slit direction) and its relative depth information are detected in parallel, providing an x–z (or y–z) profile of the sample. Thus a wavelength whose focal plane lies directly on the surface of the sample will have a maximum detected intensity, corresponding to a single horizontal position with the brightest spot on the detector. Images are subsequently stored in the computer by a frame grabber board (Dipix FPG-44) and then processed to perform quantitative measurements, as discussed in the following sections.

3. Microscope System Calibration and Characterization

The CSCM system introduced above can be used to acquire depth-profile information in parallel. Quantitative measurements can be made once proper calibration procedures as well as analysis are performed on the microscope system of Fig. 1 in terms of such characteristics as measurement sensitivity, depth field of view, and depth resolution.

A. System Calibration

Each pixel position of the CCD image, captured by the CSCM, is related to an actual two-dimensional position (x, z) on the measured sample surface. To translate raw data images into quantitative depth values, we must calibrate the scale of the CSCM by mapping the relationship between the CCD pixel coordinate and the physical surface-depth position. The calibration procedure used a flat mirror that was translated in the depth direction. At every mirror position the actual distance moved was registered, and the corresponding power spectrum, taken from the intensity image, was recorded by the CCD camera. Each row of the CCD image (1–480) now contains the spectral/depth information for each position along the imaged slit. Next, the spectral information from each row was individually processed where we calculated the center-of-mass position of the spectral intensity profile and then related the calculated pixel location to the corresponding mirror depth. This calibration procedure was car-

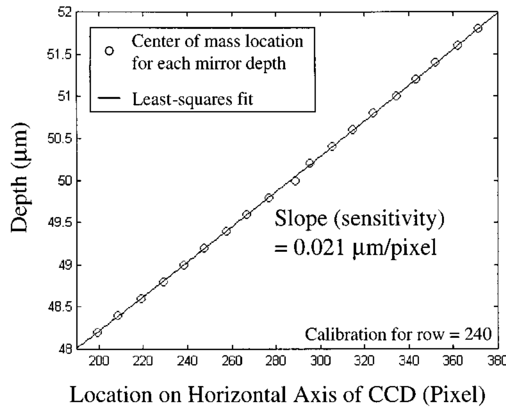

Fig. 2. Calibration lookup table for depth-to-pixel coding and sensitivity for row 240.

ried out for every row, resulting in an array of calibration lookup tables where each row has its own depth-to-pixel encoding. As an example, a lookup table for row 240 is plotted in Fig. 2, demonstrating a high linearity in the wavelength-to-depth coding characteristic of our CSCM system. Only the horizontal pixels ranging from 180 to 380 were used in calibration and measurements. Once the microscope is calibrated, we can find the quantitative depth-section measurements of any sample by first capturing the raw CCD image, performing the center-of-mass calculation to locate its pixel position, and finally determining the corresponding depth value from the calibration lookup tables. We also calibrated the transverse magnification of the CSCM system by simply translating a marker along the vertical direction and relating its position in physical coordinates to that seen in the image plane.

B. Measurement Sensitivity

Sensitivity is an important characteristic that needs to be analyzed and optimized to meet application requirements in terms of the microscope depth resolution. The example of the calibration curve shown in Fig. 2 has a sensitivity (i.e., slope) value of 21 nm/pixel when the CSCM system uses a 100× microscope objective (Leitz Wetzlar NPL Fluotar). We define the system sensitivity by the ratio $\Delta z_\lambda/\Delta x_\lambda$, where Δz_λ is the variation in the object depth direction and Δx_λ is the corresponding variation in the CCD image coordinate. In general, the system sensitivity is determined by the resolving power of the optical components used in the imaging system. For our CSCM system the sensitivity will be limited by such characteristics as the magnification power of the MO, the dispersion strength of the diffractive lens, the spectral resolving power of the monochromator, and the spatial resolution of the CCD camera.

Assuming that we use a broadband source but with a wavelength range that is small compared with the center wavelength [i.e., $(\lambda - \lambda_c) \ll \lambda_c$], the dispersion strength of a diffractive lens can be considered to be linear, following[11]

$$\frac{\Delta f_\lambda}{\Delta\lambda} = \frac{f_\lambda - f_{\lambda_c}}{\lambda - \lambda_c} \cong -\frac{f_{\lambda_c}}{\lambda_c}, \tag{1}$$

where λ and λ_c are the operating and the center wavelengths, respectively, and f_λ and f_{λ_c} are the focal lengths of the diffractive lens at the operating and the center wavelengths, respectively. The wavelength-to-depth coding of the microscope is demagnified further by the telecentric imaging from the various foci of the diffractive lens to the sample surface. Using the Gaussian lens formula and Eq. (1), we find that

$$\frac{\Delta z_\lambda}{\Delta\lambda} = \left(\frac{f_{\mathrm{MO}}}{f_{\mathrm{coupling}}}\right)^2 \frac{\Delta f_\lambda}{\Delta\lambda} \cong -\left(\frac{f_{\mathrm{MO}}}{f_{\mathrm{coupling}}}\right)^2 \left(\frac{f_{\lambda_c}}{\lambda_c}\right), \tag{2}$$

where Δz_λ is the demagnified deviation of the focal depth at the operating wavelength from that at the center wavelength, and f_{MO} and f_{coupling} are, respectively, the focal lengths of the MO and the coupling lenses, which form the telecentric imaging setup.

Next we find the dependence of the sensitivity of the CSCM on the spectral resolving power of the monochromator by evaluating the spectral position in the CCD image to wavelength variation, yielding

$$\frac{\Delta x_\lambda}{\Delta\lambda} = F_{\mathrm{FT}}\nu_0, \tag{3}$$

where Δx_λ is the variation in the position of the spectrum image intensity in the CCD plane caused by the wavelength variation $\Delta\lambda$ from the center wavelength. F_{FT} is the focal length of the Fourier-transform lens used in the monochromator, and ν_0 is the spatial frequency of the grating used in the monochromator. Finally, we obtained the sensitivity of the CSCM by combining Eqs. (2) and (3), yielding

$$\frac{\Delta z_\lambda}{\Delta x_\lambda} \cong -\frac{1}{F_{\mathrm{FT}}\nu_0}\left(\frac{f_{\mathrm{MO}}}{f_{\mathrm{coupling}}}\right)^2 \left(\frac{f_{\lambda_c}}{\lambda_c}\right). \tag{4}$$

C. Depth Resolution

Depth resolution is the second important parameter of the CSCM system, characterizing its ability to distinguish between various depth positions. The depth resolution of the CSCM is determined by the sensitivity of the measurement as well as the signal-to-noise ratio of the detection process. Assuming an ideal detection process, where the detector (i.e., the CCD camera) possesses infinite dynamic range without any noise, the center-of-mass method used to define the depth position of the measured sample surface will provide an arbitrarily high depth resolution.

However, in practice, the detected CCD image will be affected by various noise sources such as the photon noise of the optical source and the shot noise of the photodetector. The detection noise in turn will create uncertainty in determining the location of the calculated center of mass, reducing the depth resolu-

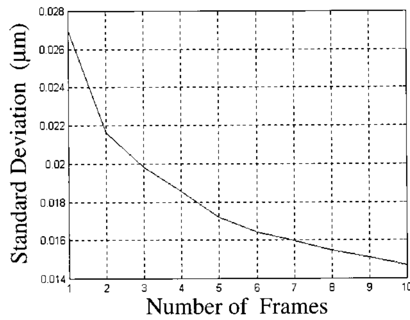

Fig. 3. Plot of measured resolution versus number of integrated frames.

tion of the CSCM. For example, the effect of detection noise is evident from our flat mirror calibration of the CSCM (see Fig. 2), where the experimentally determined center-of-mass locations deviate (i.e., scatter) from the ideal linear curve.

By assuming a uniform depth resolution over the transverse field of view, we are able to determine experimentally the depth resolution of the CSCM system by measuring a flat mirror sample. At a fixed mirror position we detected a CCD image and then applied the center-of-mass calculation on the spectral intensity profile for each position along the slit. We then mapped the resulting center-of-mass coordinates by using the calibration lookup tables (e.g., see Fig. 2) to a corresponding depth position. This measurement data are fit to a linear curve by use of a least-squares analysis, and the depth resolution of the CSCM is then determined by the value of the standard deviation from the linear curve. To improve the depth resolution, we need to increase the signal-to-noise ratio in the detected CCD image. The photon noise is multiplicative noise, and we can reduce its level by increasing the stability of the illumination source. Detector noise and quantization errors are sources of additive noise that can be reduced by increasing the intensity level of the illumination source and the dynamic range of the detection process. Indirectly, the signal-to-noise ratio degradation due to additive noise can be improved by integration of multiple frames captured by the CCD camera. Figure 3 shows the measured depth resolution (i.e., the standard deviation from linear fit) versus the number of integrated frames, demonstrating dramatic improvement in resolution for the first few frames of integration and leveling off with a further increase in the number of integrated frames. In our CSCM (the MO of 100×) experiments with the CCD camera set at 1/60 s/frame and 10-frame integration, we obtain the measured depth resolution of ~23 nm for a flat mirror sample, which is close to the pixel sensitivity measurement of 21 nm/pixel.

D. Depth Field of View

The field of view in the depth direction seen by the CSCM system is inversely proportional to the measurement sensitivity. It is also limited by the design of the microscope objective lens, the space–bandwidth product of the CCD camera, the CCD resolution, and the grating frequency. The design of the microscope objective lens is commonly optimized for a single depth position, so that any object deviation from this optimum depth position will result in image distortions in both the transverse and the longitudinal directions. We have observed such distortion from our calibration measurements when a flat mirror was scanned in the depth direction. When the mirror is scanned out of the optimal focal plane range in the longitudinal direction, we observe, as expected, that not only does the depth point-spread function become wider but also the transverse field of view is cut off. For a fixed space–bandwidth product of the CCD array, the spectral resolution of the grating affects both the sensitivity and the depth field of view (e.g., a higher spectral resolution of the grating provides higher measurement sensitivity but at the expense of reducing the depth field of view). The maximum depth field of view ΔZ can be estimated by the summation of Eq. (4) over the pixels of the CCD camera:

$$\Delta Z \cong -\frac{1}{F_{\mathrm{FT}}\nu_0}\left(\frac{f_{\mathrm{MO}}}{f_{\mathrm{coupling}}}\right)^2\left(\frac{f_{\lambda_c}}{\lambda_c}\right)\Delta X, \tag{5}$$

where we introduce $\Delta X = \Delta x_{\mathrm{pixel}} N$ with N being the number of pixels in the CCD array and $\Delta x_{\mathrm{pixel}}$ being the pixel width. For example, in our design of the CSCM system (see Fig. 1) we have ~400 effective pixels available across the full range of 640 pixels in the CCD. The reduced number of effective pixels compared with the full range is due to the broadened width of the wavelength spread in the depth image before the center-of-mass calculation is applied. Since the center-of-mass technique requires a certain spectral image width for computation, the effective range of pixels is reduced by the width of the intensity profile. Thus, with a sensitivity of 21 nm/pixel while using a 100× MO, we obtain a depth field of view of 8.4 μm for the CSCM.

4. Experimental Measurements

When the center-of-mass technique is used to locate the surface position of a sample from its spectral intensity profile, the microscope is able to provide quantitative depth-profile measurements with high depth sensitivity. In Fig. 4 we show a captured raw CCD image obtained from using the CSCM setup (MO of 100×) to measure a four-phase-level diffractive optical element that has been gold-plated to improve surface reflectivity. The figure is an image taken by the CCD rotated 90° counterclockwise to allow us to visualize the sample surface as being on top. In this case the depth (i.e., wavelength) information of the sample is contained along the y axis of the image, whereas the x axis corresponds to the transverse coordinate (i.e., the image of the sample along the slit direction) for which the depth profile is being measured. From the CCD image we first calculated the center-of-mass position for each transverse (x-axis) coordinate on the sample. We then

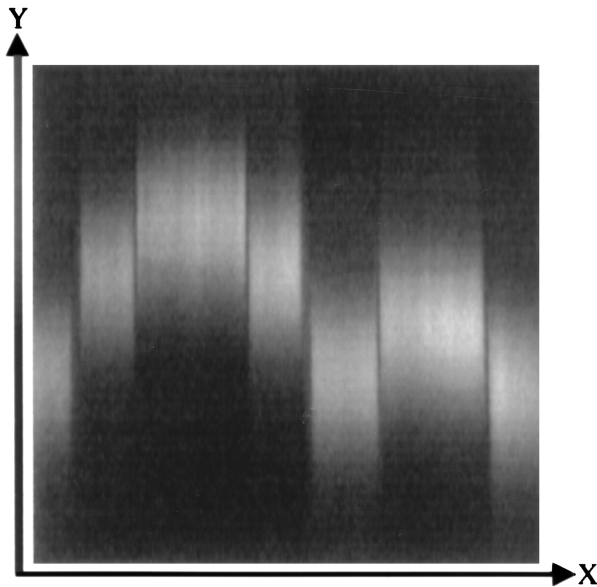

Fig. 4. Experimentally acquired raw CCD image from the CSCM applied to a four-phase-level diffractive element sample.

converted this location to a quantitative depth value by using the previously determined calibration lookup tables. In Fig. 5 we plot the depth profile of the measured sample (i.e., the depth versus transverse position along a line on the sample) found from the CCD image of Fig. 4. For comparison we summarize in Table 1 the experimental results from using three different methods for measuring the depth profile of the same diffractive optical element: our CSCM system, the Dektak profilometer, and the Zyco white-light interferometric profilometer. The measured values are consistent (with a slight discrepancy that may occur because of the uncertainty in location on the sample where the profile measurement was made), indicating that the performance of our method is comparable with other existing techniques. However, in terms of speed, the CSCM system is far superior compared with the other methods; with our method the entire depth-profile measurement is performed in a single shot and without mechanical scanning of either the probe or the sample.

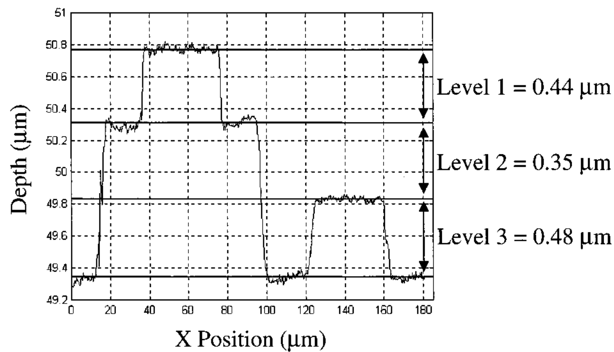

Fig. 5. Experimental depth-section profile measurement calculated for a four-phase-level diffractive element (from Fig. 4) at a CSCM resolution of 0.023 μm.

Table 1. Comparison of Profile Measurements of a Four-Phase-Level Diffractive Element (from Fig. 4) using CSCM, Dektak, and Zyco Systems

Profilometer	Level 1 (μm)	Level 2 (μm)	Level 3 (μm)
CSCM	0.44	0.35	0.48
Dektak	0.448	0.400	0.446
Zyco	0.448	0.389	0.447

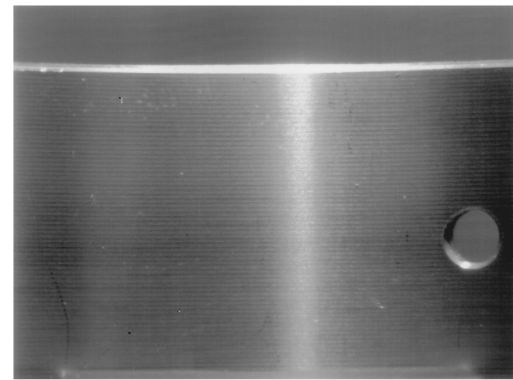

(a)

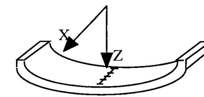

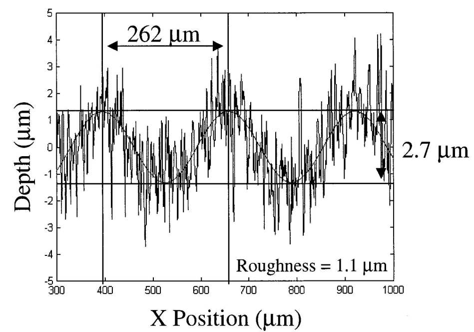

(b)

Fig. 6. (a) Magnified photograph of a machined, metal bearing. (b) Experimental measurement of a bearing where concatenated images taken by the CSCM are used.

In addition, not only does signal processing improve the CSCM sensitivity beyond the resolution limit, but it can also be used to perform many other functions useful in profilometry. For example, a machined, metal bearing shown in Fig. 6(a) has been measured with a 20× MO. The periodic grooves evident in the photograph are formed as a result of the repetitive milling process and are large compared with the groove depths. Four separate measurements have been concatenated into one plot in Fig. 6(b) to obtain the depth sensitivity and the field of view necessary to characterize this object. Further processing allowed us to characterize the periodic groove shape, called waviness, and the irregular sur-

face roughness. A superposition of the waviness profile, found when a low-pass filter is applied to the measurement data, is also plotted in Fig. 6(b). We measured a groove spacing of 262 μm with a 2.7-μm peak-to-peak depth height. By subtracting the waviness pattern from the original measurement, one can extract surface roughness where statistical analysis provides a standard deviation value for the surface roughness equal to 1.1 μm.

5. Conclusion

A CSCM system has been described that provides several advantages and new features by allowing single-shot, depth-section profiles to be acquired. Real-time measurements are possible owing to its single-shot imaging capability. In addition, the CSCM method does not require any mechanical scanning movement, since all data are acquired at the same time in parallel. This high-speed, parallel operation characteristic of the CSCM alleviates the difficulty of performing measurements in realistic environments by reducing the need for developing specially designed vibration-controlled platforms. Furthermore speed and stability of the CSCM system are achieved while the advantage of high depth sensitivity as seen in conventional confocal microscopy is maintained. By using the chromatic dispersion of a diffractive lens, our microscope dramatically improves the technique of chromatic scanning with refractive lenses. The design of the diffractive lens has been shown to be material independent, allowing the CSCM system to be built with high reproducibility. We exploit a simple design where most of the components used in the microscope come from cost-effective, off-the-shelf commercial products. With these features, the single-shot confocal microscope that we designed can serve as an effective tool for profilometry in many new fields and environments in research or in industry.

Many possible improvements to the design and applications of this system are being considered. We plan a real-time functionality for development, using a high-speed digital camera for faster than video-rate measurements and also a high-power pulsed white-light source, where we take advantage of the broadband spectrum and high intensity for shorter integration times. To modularize the CSCM while concurrently optimizing the illumination efficiency, we are investigating the implementation of fiber bundles for source and detector coupling. Furthermore, continued analyses of various sample types and application to biological imaging are being pursued.

In summary, we have shown that a CSCM can acquire high-sensitivity, depth-section profiles of a sample surface in a single shot. A method of combining a transverse slit-scan technique with a depth-scan technique that uses chromatic dispersion from a diffractive lens permits parallel measurements. This microscope has been used to measure various samples with results in good agreement with values obtained from using commercial profilometers. Characterization and optimization of the microscope and signal processing methods have also been discussed.

The authors thank Fang Xu and Rob Stein for fabrication and design of the diffractive lens and also for measurement of samples on the Dektak and Zyco systems. This research is supported by the National Science Foundation and Defense Advanced Research Project Agency.

References

1. M. Minsky, "Microscopy apparatus," U.S. patent 3,013,467 (19 December 1961).
2. J. B. Pawley, *Handbook of Biological Confocal Microscopy* (Plenum, New York, 1989).
3. S. G. Anderson, "Confocal laser microscopes see a wider field of application," Laser Focus World **30**(2), 83–86 (1994).
4. M. Bertero, P. Boccacci, R. E. Davies, and E. R. Pike, "Superresolution in confocal scanning microscope: III. The case of circular pupils," Inv. Prob. **7,** 655–674 (1991).
5. D. K. Hamilton, T. Wilson, and C. J. R. Sheppard, "Experimental observations of depth-discrimination properties of scanning microscopes," Opt. Lett. **6,** 625–626 (1981).
6. T. Wilson and C. Sheppard, *Theory and Practice of Scanning Optical Microscopy* (Academic, London, 1984).
7. D. K. Hamilton and T. Wilson, "Surface profile measurement using the confocal microscope," J. Appl. Phys. **53,** 5320–5322 (1982).
8. G. Q. Xiao, T. R. Corle, and G. S. Kino, "Real-time confocal scanning optical microscope," Appl. Phys. Lett. **53,** 716–718 (1988).
9. C. J. R. Sheppard and X. Q. Mao, "Confocal microscopes with slit apertures," J. Mod. Opt. **35,** 1169–1185 (1988).
10. G. Molesini, G. Pedrini, P. Poggi, and F. Quercioli, "Focus-wavelength encoded optical profilometer," Opt. Commun. **49,** 229–233 (1984).
11. M. C. Hutley and R. F. Stevens, "The use of a zone-plate monochromator as a displacement transducer," J. Phys. E **21,** 1037–1044 (1988).
12. S. Dobson, P. C. Sun, and Y. Fainman, "Diffractive lenses for chromatic confocal imaging," Appl. Opt. **36,** 4744–4748 (1997).